Ν

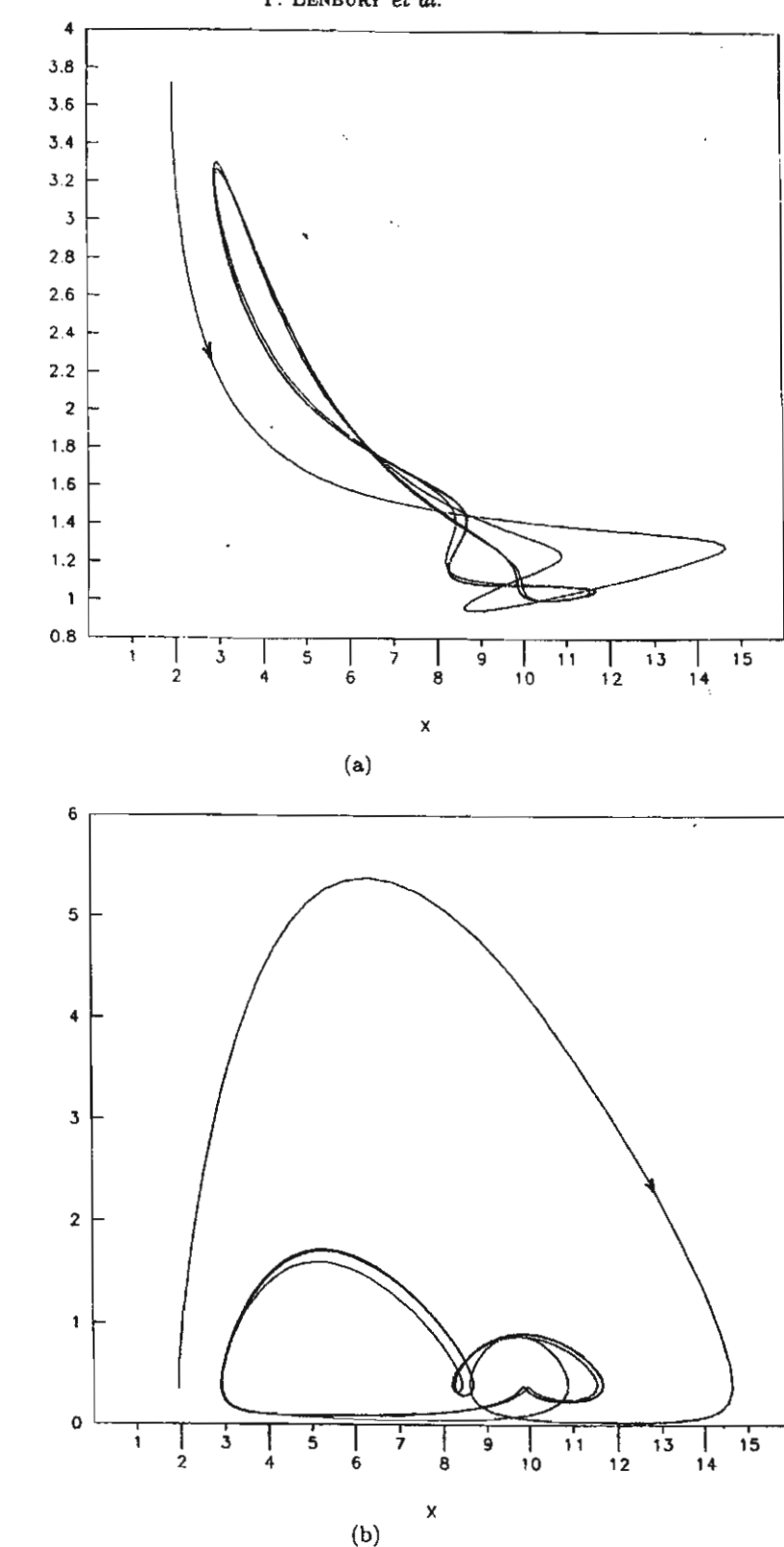


Figure 1. Computer simulation of model equations (10)–(14) with $\alpha=1.1$, $\beta=1.5$, $\rho=11$, $\eta=6$, $\delta=0.241$, M=2, $\omega=1.256$, $z_0=0.2$, $z_S=0.5$, $y_S=1.5$, and $z_S=0.05$. The solution trajectory approaches and eventually lies on a 2-torus, seen here projected onto the coordinate planes.

and finally, $\lambda_3 = -1 < 0$. Thus, all requirements for Hopf bifurcation are met. For δ in some open interval $(\delta_C, \delta_C + \varepsilon)$, the system of equations (10)–(12) with $\omega = 0$ will have a periodic solution bifurcating from its steady state (x_S, y_S, z_S) . For the system of equations (10)–(14) with $\omega \neq 0$, this means that if conditions (26) and (27) are satisfied, a Hopf bifurcation occurs on top

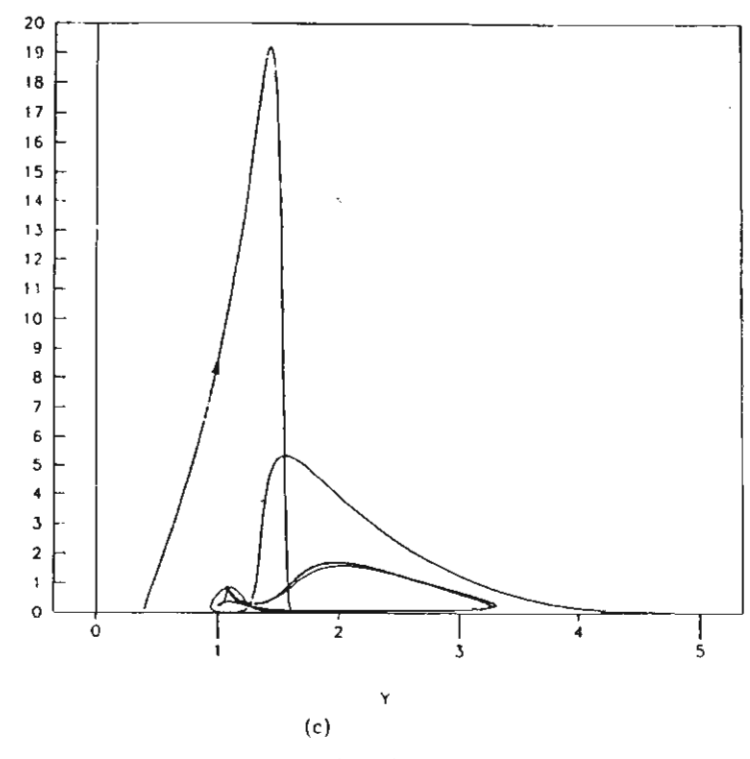


Figure 1. (cont.)

of the existing periodic solution, due to the eigenvalues $\pm i\omega$, giving rise to solution trajectories on a 2-torus in the five-dimensional phase space.

Now, with the above choice of parametric values, Hopf bifurcation occurs at a nonwashout steady state (x_S, y_S, z_S) , namely $y_S = \beta > 0$, and from (20),

$$z_S = z_0 + (\rho - \beta x_S) > 0,$$

while $x_S > 0$ by (27). In fact, the solution trajectory of the model equations (10)-(12) remains in the first octant $(x \ge 0, y \ge 0, z \ge 0)$ of the (x, y, z) space since, on substituting z = 0 into equation (12), we find

$$\frac{dz}{dT} = z_0 > 0, (28)$$

here. Also, on the (x, z) plane y = 0 so that

$$\frac{dy}{dT} = \beta > 0,$$

and on the plane x = 0, we have

$$\frac{dx}{dT} = 0,$$

so that the solution trajectory does not cross the coordinate planes.

In Figure 1, we present a computer simulation of the model equations (10)-(14) with $\omega \neq 0$ and parametric values chosen to satisfy the bifurcation requirements (26) and (27), that is, $\eta = 6$, $\beta = 1.5 = y_S$, $x_S = 0.5$, and $\rho = 11$. Then, from (25), we find

$$\delta_C = 0.125.$$

Thus, we chose $\delta = 0.241 > \delta_C$, which gives $z_S = 0.05$, M = 2, while $\omega = 1.256$, $\alpha = 1.1$, and $z_0 = 0.2$. The solution trajectory is observed to approach the closed curve on the surface of a 2-torus surrounding the steady state $(x_S, y_S, z_S, u_S, v_S) = (0.5, 1.5, 0.05, 0, 0)$ in the 5-dimensional phase space, seen here projected onto the coordinate planes.

4. FORCE FIELD INTENSITY AND BIFURCATION DIAGRAM

We now investigate the influence of the force field intensity α on the dynamic behavior of the model system (10)-(14) by first showing that the smaller the force field intensity α , the closer to the plane $y = \beta$ will the solution trajectory on the 2-torus lie.

Letting

$$G(T) \equiv \frac{\eta z(T)}{z(T) + M},\tag{29}$$

we see by (28) that G(T) > 0 for all T. Thus, equation (12) can be written as

$$\frac{d(y-\beta)}{dT} = [-\alpha u - G(T)](y-\beta) - \alpha \beta u. \tag{30}$$

Using the Leibnitz' formula, we then find

$$y(T) - \beta = e^{\int_0^T (-\alpha u - G(\tau))d\tau} \left\{ \int_0^T e^{-\int_0^T (-\alpha u - G(u))du} (-\alpha \beta u)d\tau + C \right\}. \tag{31}$$

Letting

$$h(T) = \int_0^T G(\tau) d\tau, \tag{32}$$

it is easily seen that h(T) is an increasing function, and therefore, we have

$$y(T) - \beta = e^{-\alpha v(T) - h(T)} \left\{ C - \alpha \beta \int_0^T e^{\alpha v(\tau) + h(\tau)} u(\tau) d\tau \right\},\,$$

where $e^{-h(T)} \to 0$ as $T \to \infty$.

Since $e^{h(\tau)} \leq e^{h(T)}$, $0 \leq \tau \leq T$, we have

$$\left|e^{-\alpha v(T)-h(T)}\int_0^T e^{\alpha v(\tau)+h(\tau)}u(\tau)\,d\tau\right| \leq e^{-\alpha v(T)-h(T)}e^{h(T)}\left|\int_0^T e^{\alpha v(\tau)}u(\tau)\,d\tau\right| = 1.$$

Therefore,

$$|y(T) - \beta| \le \alpha \beta$$
, as $T \to \infty$, (33)

which means that for small α , the time course of y(T) tends to a value close to β as time passes. In fact, if $\alpha = 0$, then we have

$$y(T) \to \beta$$
, as $T \to \infty$,

and the bifurcating solution trajectory eventually lies on the plane $y = \beta$. The expression (33), in fact, gives us a bound for the extent to which y will be perturbed from the value β .

Now, we have shown that the critical point (x_S, y_S, z_S) of the system of equations (10)–(12) with $\omega = 0$ loses its stability and a Hopf bifurcation occurs when the two complex conjugate eigenvalues λ_1 and λ_2 cross the imaginary axis. In other words, at the value δ_C of our bifurcation parameter δ , the two eigenvalues λ_1 and λ_2 have a vanishing real part. Figure 2 shows the stability region in the (x_S, δ) plane for a continuous stirred tank reactor modelled by equations (10)–(14) under the conditions $\beta = 1.5$, $\rho = 11$, and $\eta = 6$. The region is the union of two sets S_1 and S_2 , where

$$S_1 = \{(x_S, \delta) \mid 0 < x_S < \rho \beta^{-1}, 0 < \delta < \delta_C\},$$

$$S_2 = \{(x_S, \delta) \mid \rho \beta^{-1} < x_S\}.$$

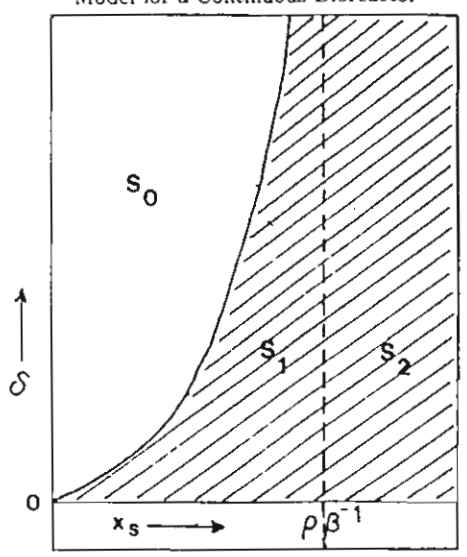


Figure 2. Stability diagram in the (x_S, δ) plane for the model system (10)-(14).

In $S_1 \cup S_2$, solution trajectories near the steady state solution $(x, y, z) = (x_S, y_S, z_S)$ remain close to that point as time passes.

On the other hand, in the instability region given by

$$S_0 = \{(x_S, \delta) \mid 0 < x_S < \rho \beta^{-1}, \delta_C < \delta < \infty\},$$

the reactor can exhibit bifurcation or chaotic behavior. The set is thus to be avoided from a control point of view. The transition from periodic orbits to chaos is known to occur after a cascade of period doubling, followed by the appearance of chaos windows. Following the work presented by Schaffer [14] on how nonlinear dynamics can elucidate mechanisms in ecology and epidemiology, we create a bifurcation diagram, shown in Figure 3, in the following manner. For each value of the force field intensity α , the simulation of the model equations (10)-(14), for parametric values in the region S_0 , is allowed to run for a sufficiently long period of time, then 40 data points $z(t_n)$, $n=1,2,\ldots,40$, are collected every interval of $2\pi/\omega$, the period of the external force field. That is,

$$T_n = T_0 + \frac{2n\pi}{\omega}, \qquad n = 1, 2, \dots, 40,$$

where $T_0=100$ in Figure 3. The values $\xi_n=\log z(T_n),\ n=1,2,\ldots,40$, are then plotted against α which ranges from 0 to 3. All other parametric values are the same in all computer simulations which generate the points in this figure. We see here that the solution is periodic for small α ; all 40 data points for each value of α apparently fall on the same spot in the (α,ξ) plane. Windows of chaos are observed for α in the approximate ranges $1.2 < \alpha < 1.9$ and $2.1 < \alpha < 3$, although the chaotic scatter of data points is more pronounced in the second range. The data points for each value of α no longer fall on the same spot, a characteristic which is markedly different from the behavior in the range where α is small.

In Figure 4, we investigate the behavior in the range $2.1 < \alpha < 3$ more closely. Here, we plot

$$H_n \equiv \xi_n - \frac{M_\alpha + m_\alpha}{2}, \qquad n = 1, 2, \dots, 40,$$

where

$$M_{\alpha} = \max_{n} \xi_{n}, \qquad m_{\alpha} = \min_{n} \xi_{n},$$

against α . We observe that at $\alpha = 2.1$, approximately, the 40 data points apparently fall on the same spot. As α increases, however, they bifurcate into two groups, one of which bifurcates

46

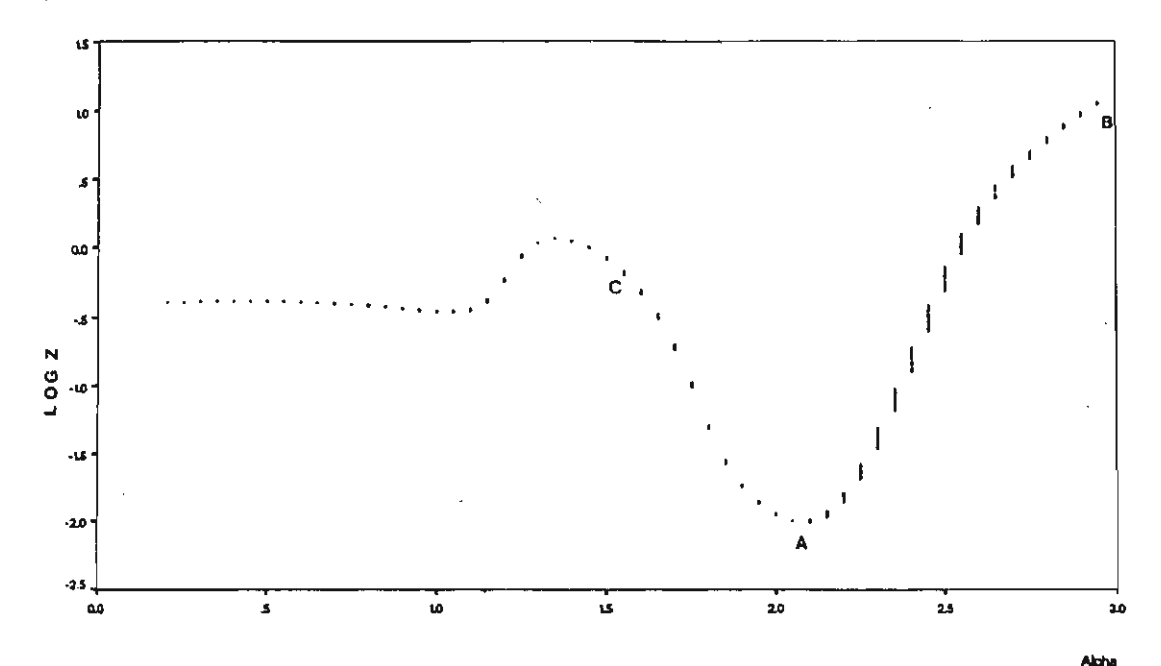


Figure 3. Bifurcation diagram of the model system (10)-(14) with parametric values in the region S_0 ; $\beta=1.5$, $\rho=11$, $\eta=6$, $\delta=0.241$, M=2, $\omega=1.256$, $z_0=0.2$, $x_S=0.5$, $y_S=1.5$, $z_S=0.05$: plot of $\log(z_n)$ versus α .

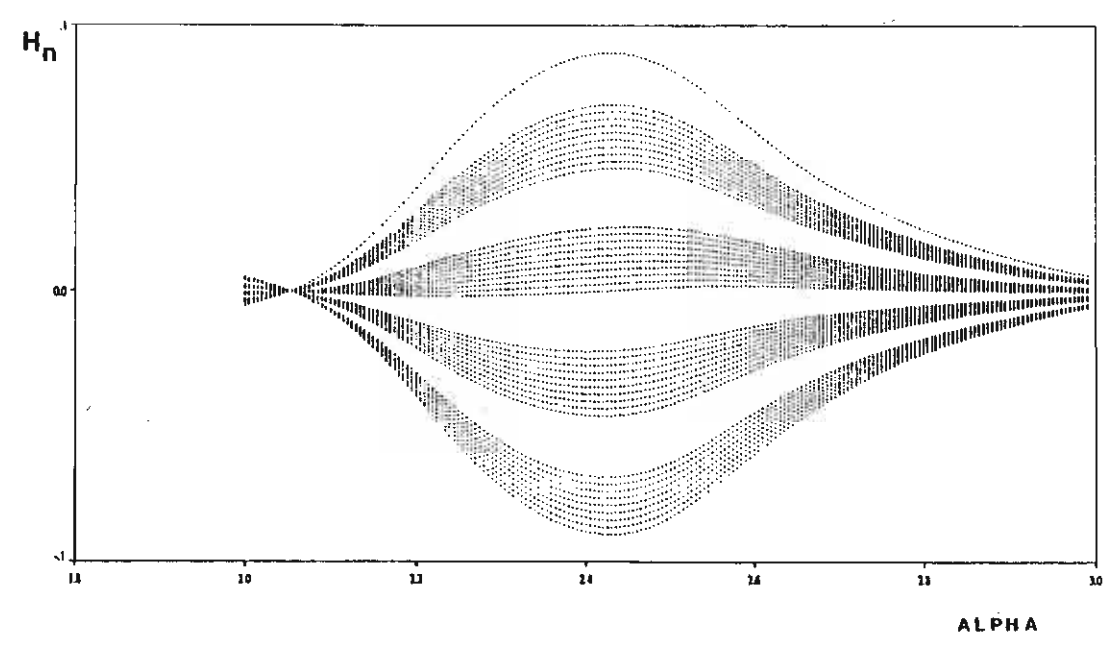


Figure 4. Bifurcation diagram of the CSTR modelled by equations (10)-(14) in the range $2 < \alpha < 3$ with parametric values of Figure 3: plot of H_n versus α .

further into four. For α around 2.45, the solution is apparently no longer periodic. We do not obtain the same value of z(T) every interval of $2\pi/\omega$. A similar chaos window can be observed for α between the values 1.2 and 1.9, approximately, although not so marked. Periodicity is recaptured, however, at α around 2.1 and 3.0 (points A and B, respectively).

Finally, Figure 5 shows the time course of z(T) for parametric values of Figure 3, but with $\alpha = 1.5$, inside the range of a chaos window (point C). The solution is no longer periodic, as is born out by the bifurcation diagram in Figure 3. Similar dynamic behavior of this type has previously been observed in a model for the spread of measles reported in [14], where an increase

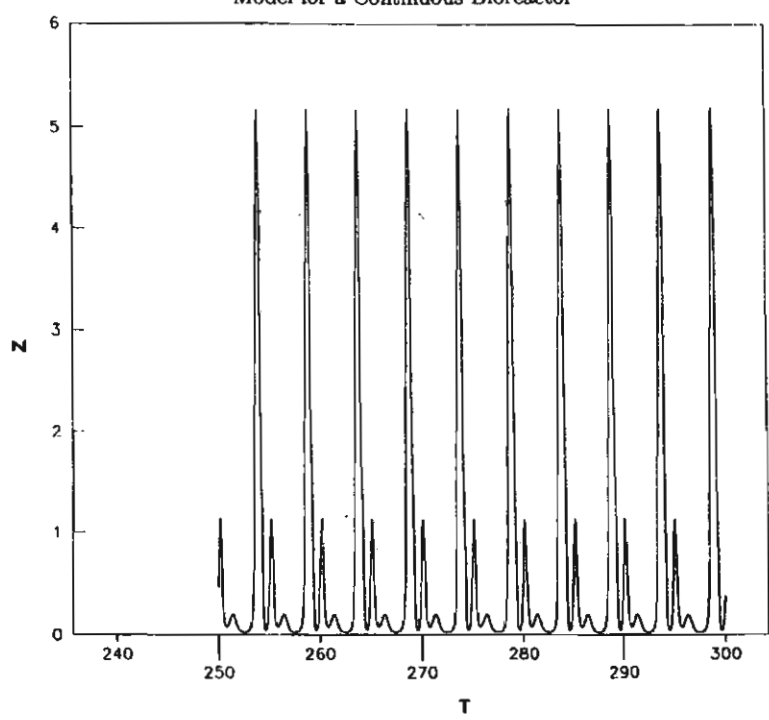


Figure 5. The time course of the simulated substrate concentration z with $\alpha = 1.5$ and other parametric values as in Figure 3.

in the amplitude of an external factor can drive the system into behaving in such an unpredictable manner.

5. CONCLUSIONS

We have investigated the dynamic behavior of a continuous stirred tank reactor modelled by cells and substrate balance equations which have been extended to incorporate the effect of external forces, such as the earth's magnetic field, on the cell membrane permeability. From considerations of the relationship between the anisotropy of the liquid crystals and the permeability of the cytoplasmic membrane, it is deduced that the membrane permeability varies with time in a sinusoidal fashion. The equation for the dynamics of variation in the permeability is then derived, taking into account also the increase in the apparent permeability due to the newly-formed cells.

The balance equation for the nutrient uptake rate is also adjusted to take into account the direct relationship between the membrane permeability and the number of active transport sites.

Bifurcation analysis done on the resulting model equations shows that, for suitable ranges of parametric values, the model system admits oscillatory behavior as a result of a Hopf bifurcation on top of the existing periodic solution due to the sinusoidal variation in the membrane permeability. Consequently, if parametric values satisfy the conditions put down in the theorem, the model system will have a solution whose phase space trajectory eventually lies on the surface of a 2-torus.

Particular attention is then devoted to the identification of the operating zones in which it is possible to carry out the continuous process while avoiding undesirable complex dynamic behavior. Owing to the importance of the process and the hazardous nature of the compounds which might be involved, we have attempted to identify the ranges of control parameters (δ and x_S , specifically) to be avoided since they correspond to the region where complex dynamic behavior is possible. The appearance of chaos windows for ranges of the external force field intensity identified in the bifurcation diagrams is not only undesirable for control and design problems, it can also give rise to potentially dangerous situations in the case where toxic compounds are involved, such as in the operation of wastewater treatment processes. Clearly, further theoret-

ical studies must be carried out to shed more light onto this complicated, but most frequently observed dynamic behavior.

REFERENCES

- 1. O. Paladino, Transition to chaos in continuous processes: Applications to wastewater treatment reactors, *Environmetics* 5, 57-70 (1994).
- 2. P. Agrawal, C. Lee, H.C. Lim and D. Ramkrishna, Theoretical investigations of dynamic behavior of isothermal continuous stirred tank biological reactors, *Chemical Engineering Science* 37, 453-462 (1982).
- 3. L. Pellegrini and G. Biardi, Chaotic behavior of a controlled CSTR, Computers and Chemical Engineering 14, 1237-1247 (1990).
- 4. J. Cheng-Fu, Existence and uniqueness of limit cycles in continuous cultures of micro-organisms with non-constant yield factor. Universita degli studi di Bari, Italy, (preprint).
- 5. T. Yano, Dynamic behavior of the chemostat subject to substrate inhibition, Biotechnology and Bioengineering 11, 130-153 (1960).
- Y. Lenbury, B. Novaprateep and B. Wiwatpataphee, Dynamic behavior classification of a model for a continuous bio-reactor subject to product inhibiton, Mathl. Comput. Modelling 19 (12), 107-117 (1994).
- L. Yerushalmi, B. Volesky, J. Votruba and L. Molnar, Circadian rhythmicity in a fermentation process, Appl. Microbiol. Biotechnol. 30, 460-474 (1989).
- 8. D.S. Thomas and A.H. Rose, Inhibitory effect of ethanol on growth and solute accumulations by Saccharomyces cerevisiae as affected by plasma-membrane lipid composition, Arch. Microbiol. 122, 49 (1979).
- 9. A.A. Herrero and R.F. Gomez, Development of ethanal tolerance in clostridium thermocellum: Effects of growth temperature, Appl. Environ. Microbiol. 40, 571 (1980).
- C.J. Panchal and G.G. Stewart, Regulatory factors in alcohol fermentations, Proc. Int. Yeast Symp. 5, 9 (1981).
- F.T. Hong, Photoelectric and magneto-orientation effects in pigmented biological membranes, J. Colloid and Interface Sci. 58, 471 (1977).
- 12. A.P. Dubrov, The Geomagnetic Field and Life, Plenum Press, New York, pp. 20-45, (1974).
- 13. J.E. Marsden and M. McCracken, The Hopf Bifurcation and its Applications, Springer-Verlag, New York, pp. 65-135, (1976).
- S. Schaffer and W.M. Can, Nonlinear dynamics elucidate mechanisms in ecology and epidemiology, IMA J. Math. Appl. Med. Biol. 2, 221-252 (1985).

1.3 แฟกเตอร์ที่สามที่ผู้วิจัยคำนึงถึงอีกแฟกเตอร์หนึ่งคือ ผลผลิต (product) ของขบวน การหมัก ซึ่งเมื่อ product นี้ มีปริมาณมากขึ้นก็สามารถมีผลทำให้อัตราการเพิ่มจำนวนของ x ลดลง ได้ เช่น ขบวนการในปฏิกรณ์ต่อเนื่อง (continuous bio-reactors) จะพบว่า product เป็นก๊าซ เช่น ethanol หรือเป็น cells killing products อื่น ๆ ซึ่งเป็นผลพวงของขบวนการนั้น ๆ จะสามารถ inhibit การเจริญเติบโต หรือการขยายพันธุ์ของ x ได้ ในขณะที่ระดับของเหยื่อ หรือสารอาหารที่มีสูงเกินไป ก็สามารถ inhibit การขยายพันธุ์ของ x ได้เช่นกัน

ผู้วิจัยจึงได้นำ model ค้นแบบ (2) และ (3) มาปรับเปลี่ยนเพิ่มเคิมสมการที่สามซึ่งคิดถึงการ เปลี่ยนแปลงในระดับของ product P(t) และได้เป็นระบบสมการไม่เชิงเส้น 3 สมการ ดังนี้

$$\frac{dS}{dt} = D(S_F - S) - \frac{\mu x}{Y}$$
 (22)

$$\frac{\mathrm{dx}}{\mathrm{dt}} = \mu \mathbf{x} - \mathbf{D}\mathbf{x} \tag{23}$$

$$\frac{dP}{dt} = \eta_0 \mu x - DP \tag{24}$$

โดยที่

$$\mu = \frac{kSe^{-\frac{S}{K_S}}}{\left\{1 + \frac{P}{K_P}\right\}} \tag{25}$$

โดยการวิเคราะห์ด้วย singular perturbation technique เราสามารถแสดงได้ว่า ถ้าเงื่อนไข ต่อไปนี้เป็นจริง

$$a > 1 \tag{26}$$

$$\beta > 1 - \frac{1}{a} - \frac{1}{a^2} \tag{27}$$

$$e^{a} < \frac{\omega}{d_{2}} < ae \left[\frac{\varepsilon \eta d_{1}}{\gamma d_{3}} \left(1 - \frac{1}{a} \right) \left(\frac{1}{a} + \beta \right) + 1 \right]$$
 (28)

ແຄະ

$$\frac{\eta d_1 \beta}{\gamma d_2} > \frac{1}{ae} \tag{29}$$

ระบบสมการ (22)-(25) จะมีคำตอบที่เป็นคาบ ซึ่งผลงานในขั้นต้นนี้ได้นำเสนอในการประชุมวิชาการ นานาชาติ International Conference on Dynamical Systems and Differential Equations ที่ Southwest Missouri State University ณ ประเทศสหรัฐอเมริกา และได้รับตีพิมพ์ใน Proceedings ของการประชมแล้ว ดังเอกสารที่ได้แนบมาต่อไปนี้

ทั้งนี้ผู้วิจัยยังได้ดำเนินการวิจัยต่อให้ละเอียด และสมบูรณ์ขึ้น แล้วนำเขียนขึ้นเป็น paper และ submitted for publication ในวารสาร Mathematical Modelling of Systems แล้ว ดังที่จะสามารถอ่าน ดูรายละเอียดของการวิเคราะห์วิจัยได้ในเอกสารที่แนบมาด้วยนี้เช่นกัน A Singular Perturbation Analysis of a Product Inhibition

Model for Continuous Bio-Reactor

A SINGULAR PERTURBATION ANALYSIS OF A PRODUCT INHIBITION MODEL FOR CONTINUOS BIO-REACTORS

Y. LENBURY Bangkok, Thailand. Department of Mathematics, Faculty of Science, Mahidol University,

N. TUMRASVIN Bangkok, Thailand.

Department of Mathematics, Faculty of Science, Mahidol University,

ABSTRACT

A model of a continuous bio-reactor subject to product inhibition is considered where a one hump substrate-limited specific growth rate is used. Analysis of the model is carried out through singular perturbation arguments which allow us to derive explicit conditions on the parameters that identify different dynamic behavior of the system, and specifically ascertain the existence of a limit cycle composed of a concatenation of catastrophic transitions occurring at different speeds. Moreover, the interactions between the limiting substrate and the growing microorganisms can give rise to high-frequency oscillations, which can arise during the transients toward the attractor or during the low-frequency cycle. This periodic burst of high-frequency oscillations develops as a result of the effective product inhibitory mechanisms. The analysis helps us in identifying the safe operating region in which undesirable complexed dynamic behavior may be avoided.

1 INTRODUCTION

Viewing the behavior of microbial cultures within the framework of lumped kinetic models, a multitude of models have been proposed and theoretically studied in diverse ways since the model due to Monod [1] fashioned after Michaelis-Menten kinetics for single enzyme-substrate reactions.

In [2], Yano and Koga made a theoretical study on the behavior of a single-vessel continuous fermentation subject to a growth inhibition at high concentration of the rate limiting substrate S. They used the following expression for their continuous fermentation system:

$$\mu = \frac{\mu_{m}}{(K_{s}/S) + 1 + \sum_{j=1}^{n} (S/K_{j})^{j}}$$
(1)

where μ_m and the K's are positive constants and n is a positive integer. Other workers [3-5] have adopted simpler specific growth rate functions involving less control parameters but exhibiting similar necessary characteristics as the usual substrate inhibition model, for example the one hump substrate inhibition function

$$\mu = kSe^{-S/K_s} \tag{2}$$

where k and K_s are positive constants.

Later, Yano and Koga discussed in [6] the nature of the chemostat in which the specific growth rate depends on the concentrations of both a substrate and an inhibitory product of a microorganism. They assumed the specific growth rate equation as follows;

$$\mu = \frac{\mu_{\rm m}S}{(K_{\rm s} + S) \left\{ 1 + \left(\frac{P}{K_{\rm p}}\right)^{\rm n} \right\}}$$
(3)

They showed, with the analog computer, that when the product formation was negatively growth-associated, diverging as well as damped oscillations appeared. No oscillations could be observed, on the other hand, when the product formation was either completely growth-associated, or partially growth-associated. Oscillation phenomena are, however, not unusual in continuous cultures [3]. Since such penchant for periodicity is undesirable from the point of view of process control, it is necessary to identify the safe operating regions in which complexed dynamic behavior may be avoided.

In [4], the dynamic behavior of a chemostat subject to product inhibition was analyzed and classified in terms of multiplicity and stability of steady states and limit cycles. The substrate was assumed to be in sufficient supply so that the model was reduced to a system of two nonlinear differential equations involving only the cells and product concentrations.

In this paper, we consider the full three-variable product inhibition model consisting of the following nonlinear differential equations (described in more detail in [6]):

$$\frac{dS}{dt} = D(S_F - S) - \frac{\mu}{Y}X$$
(4)

$$\frac{dX}{dt} = \mu X - DX \tag{5}$$

$$\frac{dP}{dt} = \eta_0 \mu X - DP \tag{6}$$

where X(t) denotes the cells concentration at time t; S(t) the substrate concentration at time t; P(t) the product concentration at time t; S_F the concentration of the feed substrate; Y the cells to substrate yield; P(t) the dilution rate; and P(t) the constant for product formation. Equations (4) and (5) are based on the well known Monod's model for cells and substrate interaction, described in more detail in reference [1]. To take into account the inhibitory effects of the substrate as well as the product increase in the chemostat, however, we adopt the following expression for the specific growth rate function:

$$\mu = \frac{kSe^{-\frac{S}{K_s}}}{1 + \frac{P}{K_p}} \tag{7}$$

Further, the cells to substrate yield Y is assumed to vary linearly with the substrate level at any time t, allowing for the positively-growth associated situation; namely

$$y = AS + B \tag{8}$$

Such substrate dependent yield has been used previously by several other workers in this field [3-5].

Equation (6) describes the change in the product concentration as X and S change. The first term on the right of this equation is the contribution to the rate of change in P, which is assumed to vary directly as the rate at which X increases, η_0 being the positive constant of variation. The cells X, substrate S, and product P are extracted from the chemostat at a constant dilution rate D, and hence the terms -DS, -DX, and -DP in the three model equations (4) through (6).

The analysis of the model is done through a singular perturbation argument, assuming that the substrate concentration exhibits fast dynamics. The time responses of the different components in the system are assumed to decrease dynamically from top to bottom. The structure of the corresponding attractors and the nature of the transients are then analyzed. It is shown that the model system can exhibit low-frequency cycles in which periodic bursts of high-frequency oscillations may develop giving rise to more complexed dynamical behavior for specified ranges of the system parameters.

2 SYSTEM MODEL

In order to analyze the model system of equations (4), (5) and (6), together with (7) and (8) through the singular perturbation technique, we scale the dynamics of the three hierarchical components of the system by means of two small dimensionless positive parameters ε and δ ;

$$\begin{split} &\text{namely, we let } x = \frac{S}{S_F}, \, y = X, \quad z = \frac{P}{\epsilon K_P} \,\,, \,\, d_1 = D, \,\, d_2 = \frac{D}{\epsilon} \quad, \,\, d_3 = \frac{D}{\epsilon \delta} \quad, \quad \omega = \frac{k S_F}{\epsilon}, \\ &\eta = \frac{\eta_0 \omega}{\epsilon \delta K_P}, \gamma = \frac{k}{A S_F} \quad, \,\, \beta = \frac{B}{A S_F} \quad, \,\, \text{and} \,\, a = \frac{S_F}{K_S} \,\,. \end{split}$$

We are led to the following system of differential equations:

$$\frac{\mathrm{d}x}{\mathrm{d}t} = d_1(1-x) - \frac{\gamma x e^{-ax} y}{(x+\beta)(1+\varepsilon z)} \equiv f(x,y,z) \tag{9}$$

$$\frac{dy}{dt} = \varepsilon y \left[\frac{\omega x e^{-ax}}{1 + \varepsilon z} - d_2 \right] \equiv \varepsilon g(x, y, z)$$
 (10)

$$\frac{dz}{dt} = \varepsilon \delta \left[\frac{\eta x e^{-ax}}{1 + \varepsilon z} y - d_3 z \right] \equiv \varepsilon \delta h(x, y, z)$$
(11)

Thus, with ε and δ small, the equation of the substrate concentration represents the fast system, while that of the cells and product concentrations represent the intermediate and the slow systems respectively. Under suitable regularity assumptions, the singular perturbation method allows us to approximate the solution of the system (9)-(11) with a sequence of simple dynamic transitions along the various equilibrium manifolds of the system and occurring at different speeds. The resulting path, composed of all such transitions, approximates the solution of the system in the sense that the real trajectory is contained in a tube around these transients, and that the radius of the tube goes to zero with ε and δ . The formal proof of this is not given because it is long and trivial and has already been discussed and extensively used in the literature [7-10].

3 EXISTENCE OF LIMIT CYCLE

We now show that if ε and δ are sufficiently small and

$$a > 1 \tag{12}$$

$$\beta > 1 - \frac{1}{a} - \frac{1}{a^2} \tag{13}$$

$$e^{a} < \frac{\omega}{d_{2}} < ae \left[\frac{\varepsilon \eta d_{1}}{\gamma d_{3}} \left(1 - \frac{1}{a} \right) \left(\frac{1}{a} + \beta \right) + 1 \right]$$
 (14)

$$\frac{\eta d_1 \beta}{\gamma d_3} > \frac{1}{ae} \tag{15}$$

then a limit cycle exists for the model system (9)-(11).

We first prove that inequalities (12)-(15) guarantee that the geometry of the manifolds f = 0, g = 0 and h = 0 is as in Fig. 1.

Manifold f = 0

We observe that this manifold is given by the equation

$$y = \frac{d_1}{\gamma} (1 - x)(x + \beta)(1 + \varepsilon z) \frac{e^{ax}}{x}$$
 (16)

which defines a surface $y = \varphi(x, z)$ which intersects the (x, y) plane along the curve

$$y = \frac{d_1}{\gamma} (1 - x)(x + \beta) \frac{e^{ax}}{x}$$
 (17)

From equation (16), it is seen that the manifold intersects the (x,z) plane along the line x = 1 as shown in Fig. 1.

The slope of the curve in (17) is given by

$$\frac{\mathrm{d}y}{\mathrm{d}x} = \frac{\mathrm{d}_1}{\gamma} \frac{\mathrm{e}^{\mathrm{a}x}}{\mathrm{x}^2} F(x) \equiv \frac{\mathrm{d}_1}{\gamma} \frac{\mathrm{e}^{\mathrm{a}x}}{\mathrm{x}^2} \Big[-x^3 + (a - a\beta - 1)x^2 + a\beta x - \beta \Big] \tag{18}$$

which may vanish for some values of x < 1.

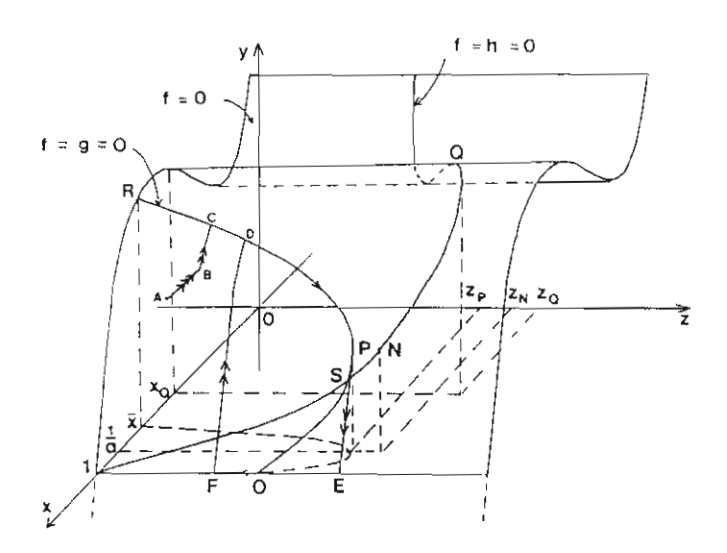


Figure 1 Equilibrium manifolds of the model system (9)-(11). In this case, transitions of different speeds develop into a closed cycle, where one, two and three arrows indicate transitions at low-, intermediate-, and high-speed, respectively.

Manifold g = 0

This manifold consists of 2 parts; the trivial manifold y = 0 and the nontrivial manifold given by the equation

$$\frac{xe^{-ax}}{1+\epsilon z} = \frac{d_2}{\omega} \tag{19}$$

which defines a surface $z = \psi(x)$. We observe that at $x = \frac{1}{a}$

$$\frac{dz}{dx} = 0$$

and so inequality (12) ensures that the point $P(x_p, y_p, z_p)$ in Fig. 1 is located on the manifold f = 0 at the point where $x_p = \frac{1}{a} < 1$.

We also need the point P to be located on the stable part of the manifold f = 0. This is guaranteed by requiring that

$$F\left(\frac{1}{a}\right) < 0 \tag{20}$$

which is equivalent to inequality (13)

The manifolds f = 0 and g = 0 intersect along the curve given by

$$y = \frac{d_1\omega}{d_2\gamma}(1-x)(x+\beta)$$

reaching a maximum at the point $M(x_M, y_M, z_M)$ where

$$x_{M} = \frac{1-\beta}{2}$$

Finally, the curve f = g = 0 intersects the (x, z) plane at the point $O(x_0, y_0, z_0)$ where $x_0 = 1$ and, from (19),

$$z_{0} = \frac{1}{\varepsilon} \left(\frac{\omega}{d_{2}e^{a}} - 1 \right) \tag{21}$$

We see, therefore, that the left side of inequality (14) guarantees that $z_0 > 0$.

Thus, the manifold f = g = 0 is shaped as shown in Fig. 1. We note that the point R may be located on the unstable part of the manifold f = 0. However, the transients also develop into a limit cycle in the case that inequalities (12)-(15) are satisfied.

Manifold h = 0

This manifold is given by the equation

$$z = \frac{\eta x y e^{-ax}}{d_3(1 + \varepsilon z)} \tag{22}$$

which defines a surface $z = \rho(x, y)$. This intersects the manifold f = 0 along the curve

$$z = \frac{\eta d_1}{\gamma d_1} (1 - x)(x + \beta) \tag{23}$$

using equation (16). Thus , z reaches a maximum along this curve at the point $Q(x_Q, y_Q, z_Q)$ where $x_Q = \frac{1}{2}(1-\beta) = x_M$

Also, the curve f = h = 0 intersects the (x,z) plane at the point (1,0,0) as seen in Fig. 1. If we let $N(x_N, y_N, z_N)$ be the point on the curve f = h = 0 with $x_N = \frac{1}{a}$, then from equation (23) we find that

$$z_{N} = \frac{\eta d_{1}}{\gamma d_{2}} \left(1 - \frac{1}{a} \right) \left(\frac{1}{a} + \beta \right) \tag{24}$$

while, from equation (19), we find that

$$z_{\mathbf{p}} = \frac{1}{\varepsilon} \left(\frac{\omega}{\text{aed}_2} - 1 \right) \tag{25}$$

Therefore, so that the equilibrium point S where the curves f = g = 0 and f = g = 0 intersect should be located on the unstable part of the manifold f = g = 0, we require

$$Z_p < Z_N$$

which is exactly the right side of inequality (14).

Finally, along this curve f = h = 0 given by equation (23),

$$z = \frac{\eta d_1}{\gamma d_3}$$

when x = 0, and therefore inequality (15) guarantees that the curve f = h = 0 crosses the curve f = g = 0 only once at the point S.

Now, starting from a point A = (x(0), y(0), z(0)) (see Fig. 1 where low-, intermediate-, and high-speed trajectories are indicated, respectively, with one, two, and three arrows) at first a high-speed transition develops at constant y and z while only the fast system

$$\dot{x} = f(x(t), y(0), z(0))$$

is active and the intermediate (y) and slow (z) variables are frozen at their initial values y(0) and z(0). The high speed transition brings the system to the point B on the stable part of the fast manifold f=0, at which point the intermediate system has now become active. A second intermediate-speed transition takes place on the manifold at constant x (segment AB in Fig. 1) until the point C is reached. A slow transition is then made along the curve f=g=0 until the point P is reached where the stability of the equilibrium manifold g=0 is lost and a quick transition then takes the state of the system to the equilibrium point E on the stable trivial manifold y=0. A slow transition then develops along this manifold until a point is reached where the stability is again lost at some point F beyond O (see Fig. 1). The proof of the existence and location of such a point F is lengthy and can be found in Schecter and Osipove et al. [11,12]. At this point a quick jump again takes us back to the point D on the stable manifold f=g=0, resulting in a closed cycle DPEF lying on the equilibrium manifold f=0.

Fig. 2 shows numerical simulation of the model equations (9)-(11) with parametric values chosen to satisfy inequalities (12)-(15). The trajectory is seen here to develop into a low-frequency limit cycle as theoretically predicted. The time courses of the three variables in this case are shown in Fig. 3.

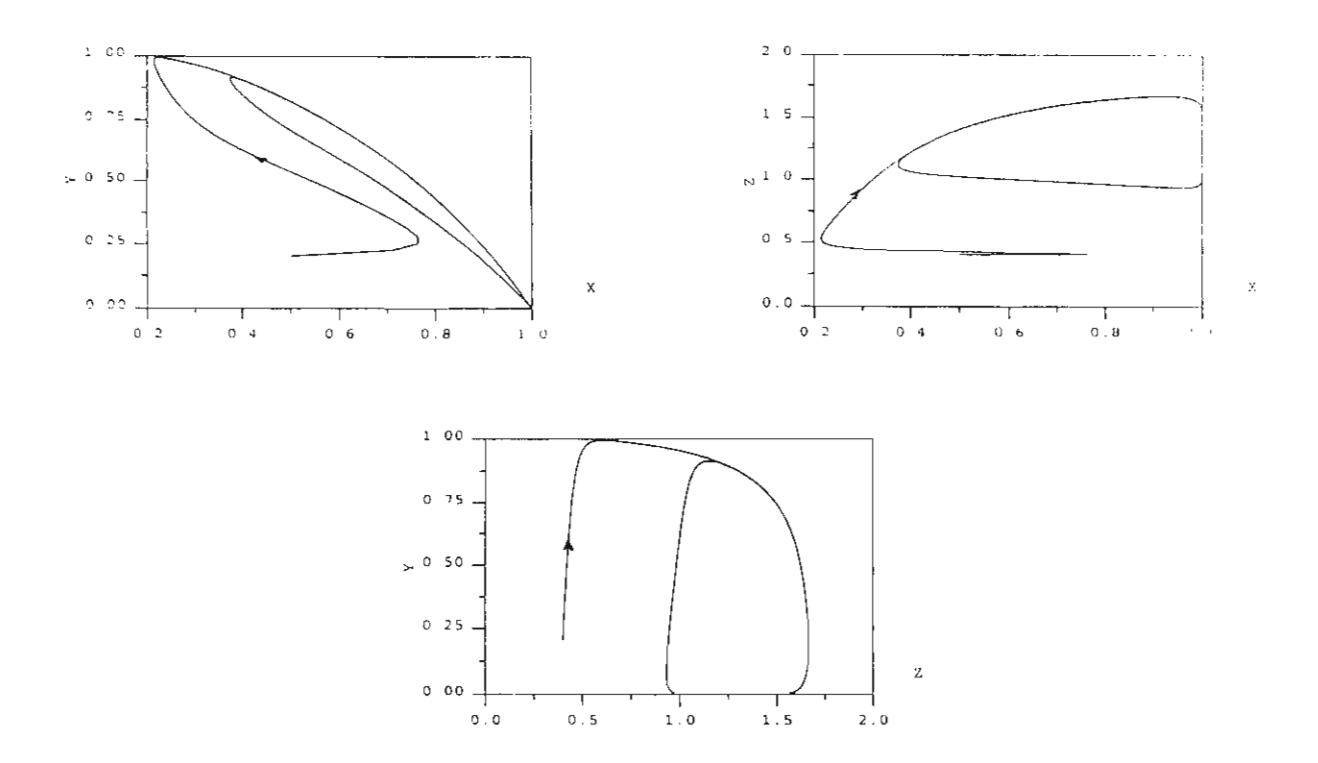
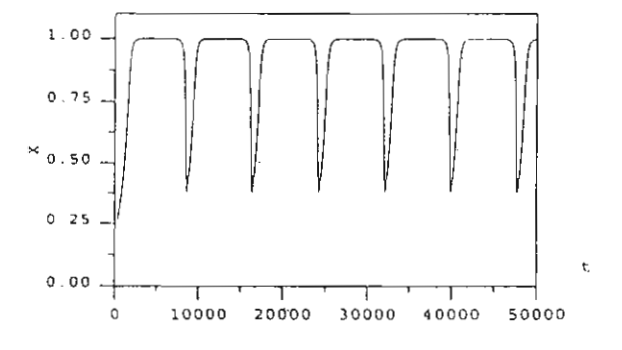
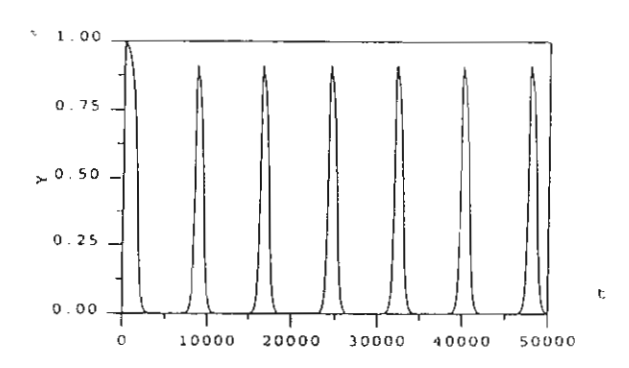


Figure 2 Numerical simulation of the model equations (9)-(11) where the parametric values have been chosen to satisfy inequalities (12)-(15), so that the solution trajectory tends toward a low-frequency limit cycle as theoretically predicted. Here, $\varepsilon = 0.1$, $\delta = 0.01$, $\beta = 0.8$, $\gamma = 2.0$, $\eta = 10.0$, $\omega = 3.0$, $\alpha = 1.5$, $\alpha = 0.25$, $\alpha = 0.3$, $\alpha = 0.1$, $\alpha = 0.1$, $\alpha = 0.2$, and $\alpha = 0.2$, and $\alpha = 0.2$, $\alpha = 0.3$, α





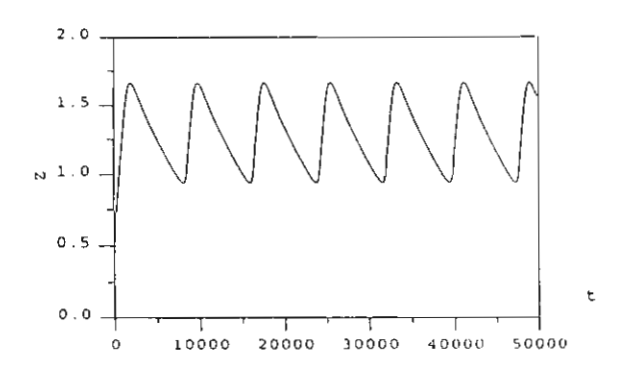


Figure 3 The time courses of the three variables x(t), y(t), and z(t) are shown here corresponding to the case seen in Fig. 2. Here, $\epsilon = 0.1$, $\delta = 0.01$, $\beta = 0.8$, $\gamma = 2.0$, $\eta = 10.0$, $\omega = 3.0$, $\alpha = 1.5$, $\alpha = 0.25$, $\alpha = 0.3$, $\alpha = 0.1$, $\alpha = 0.25$, $\alpha = 0.3$, $\alpha = 0.1$, $\alpha = 0.25$, $\alpha = 0.3$, $\alpha = 0.1$, $\alpha = 0.25$, $\alpha = 0.3$, $\alpha = 0.1$, $\alpha = 0.25$, $\alpha = 0.3$, $\alpha = 0.$

4 BURSTS OF HIGH-FREQUENCY OSCILLATIONS

For the occurrence of periodic burst of high-frequency oscillations during each low-frequency cycle, we further require that the manifold f = 0 has an unstable portion. This is equivalent to requiring that the slope given by equation (18) is positive at some value of x < 1, say $x = \frac{1}{3}$.

Letting $x = \frac{1}{3}$ in (18) leads to the following inequality

$$\beta < \frac{3a - 4}{27 - 6a} \tag{26}$$

which ensures that the curve $y = \phi(x,0)$ has positive slope on some interval containing the point $x = \frac{1}{2}$.

Combining inequalities (13) and (26) leads to the requirement that

$$1 - \frac{1}{a} - \frac{1}{a^2} < \beta < \frac{3a - 4}{27 - 6a} \tag{27}$$

It is also necessary to have

$$F(\bar{x}) > 0 \tag{28}$$

so that the point R should be located now on the unstable branch of the manifold f = 0. This is easily accomplished by letting

$$\overline{\mathbf{x}} = \frac{1}{3} - \theta \tag{29}$$

for a sufficiently small θ , then simply set

$$\frac{d_2}{\omega} = \overline{x}e^{-\overline{x}} = (\frac{1}{3} - \theta)e^{-(1/3 - \theta)}$$
(30)

Finally, in order that the transition goes back into high-frequency oscillations in each low-frequency cycle, we require $z_0 < z_M$, which is equivalent to

$$e^{-a} < \frac{1-\beta}{2} e^{-a(1-\beta)/2} \tag{31}$$

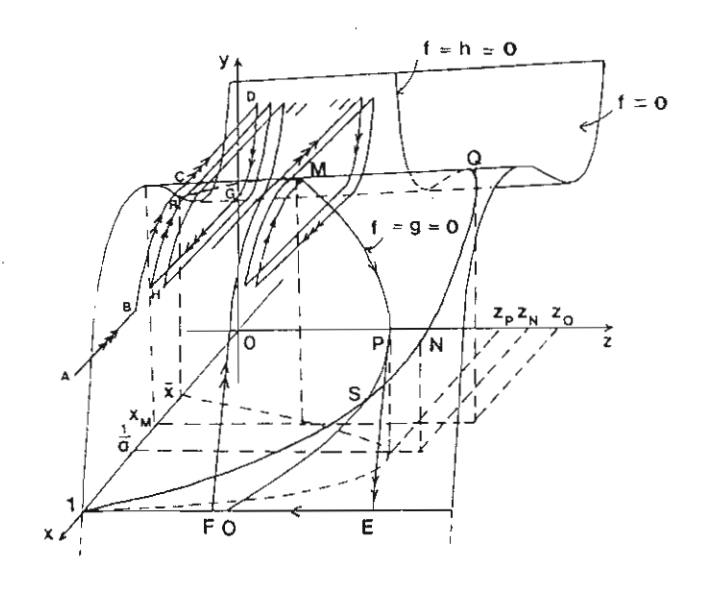


Figure 4 Equilibrium manifolds of the model system (9)-(11). In this case, transitions of different speeds develop into a low-frequency cycle with a period of high-frequency oscillation as identified in the text.

With all the above inequalities being satisfied, the equilibrium manifolds are shaped as shown in Fig. 4. Starting from the point A, a fast transition takes us, as explained earlier, to the point B on f = 0. An intermediate transition develops on this manifold until C is reached where the stability of the equilibrium fast manifold is lost. A fast transition then takes the system to the stable equilibrium point D. An intermediate speed transition is then made along this branch of manifold until G is reached where the stability is again lost and a quick jump brings us to the stable point H. This almost closes up the cycle but just misses the point B. The slow system has become active and z has been slowly increasing since $\dot{z} > 0$ here. Transitions then develop following the same pattern but with slowly varying z as seen in Fig. 4 until M is reached, at which point the trajectory develops into a slow cycle which goes back into the fast cycles since inequality (31) guarantees that $z_F < z_M$.

Thus, we have proved, by the above discussions, the following theorem

THEOREM If inequalities (12), (14), (15), (27), (30) and (31) hold then the system of equations (9)-(11) has a periodic solution which will be a low-frequency limit cycle containing high-frequency oscillations if ε , δ , and θ are sufficiently small.

Fig. 5 shows numerical simulation of the model equations (9)-(11) with parametric values chosen to satisfy all inequalities mentioned in the above theorem. The corresponding time courses of the three variables are shown in Fig. 6, where the burst of high frequency oscillations is observed in each low-frequency cycle.

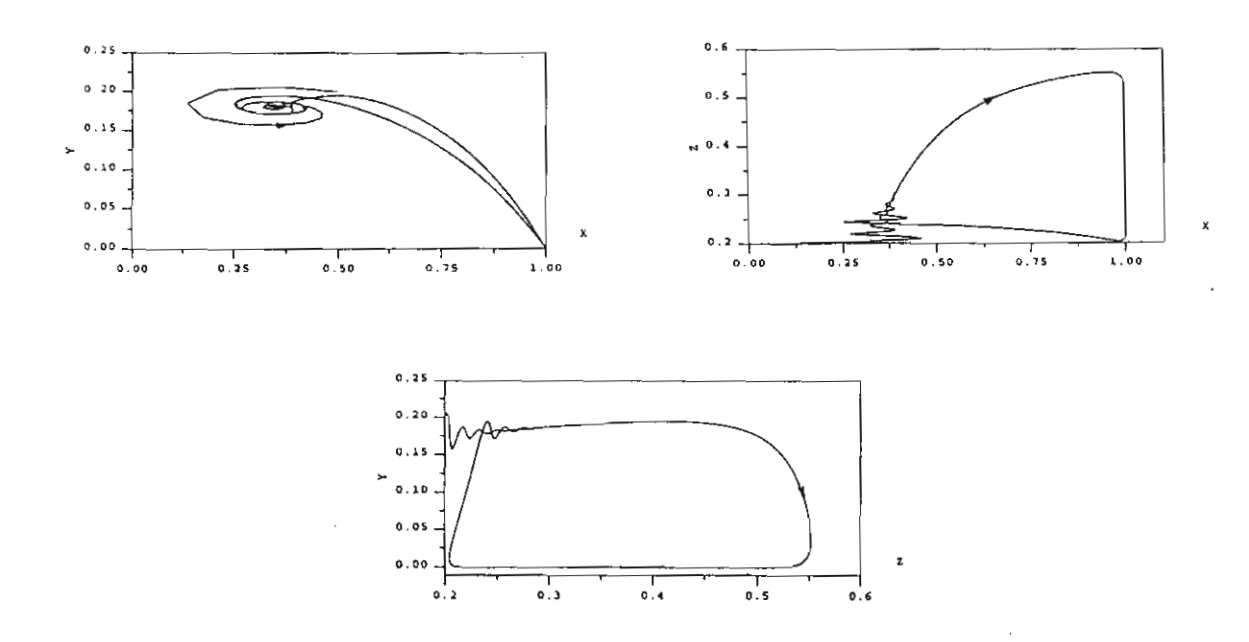
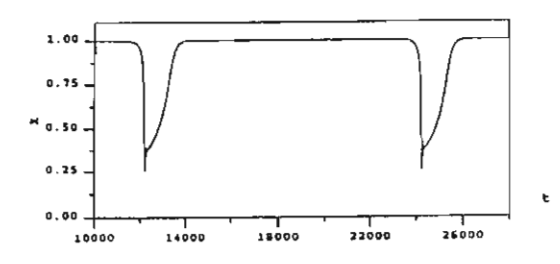
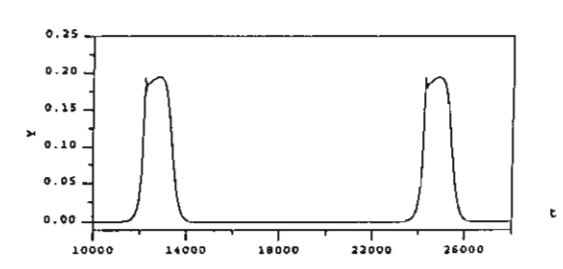


Figure 5 Numerical simulation of the model equations (9)-(11) where the parametric values have been chosen to satisfy all the inequalities set out in the Theorem. The solution trajectory is a low-frequency limit cycle which contains a period of high-frequency oscillations. Here, $\epsilon=0.1$, $\delta=0.01$, $\beta=0.02$, $\gamma=2.0$, $\eta=10.0$, $\omega=3.0$, a=1.5, $d_1=0.25$, $d_2=0.5$, $d_3=0.1$, x(0)=0.5, y(0)=0.2, and z(0)=0.2.





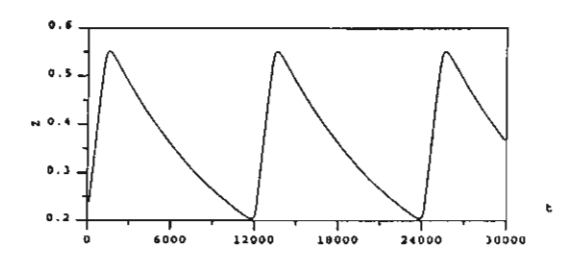


Figure 6 The time courses of the three varibles x(t), y(t), and z(t) corresponding to the case seen in Fig. 4 are shown here, where periodic bursts of high-frequency oscillations are clearly observed. Here, $\epsilon=0.1$, $\delta=0.01$, $\beta=0.02$, $\gamma=2.0$, $\eta=10.0$, $\omega=3.0$, a=1.5, $d_1=0.25$, $d_2=0.5$, $d_3=0.1$, x(0)=0.5, y(0)=0.2, and z(0)=0.2.

5 CONCLUSION

The dynamic behavior of a continuous bio-reactor described by equations (9)-(11) has been investigated in this paper. Assuming that the time responses of the three components are highly diversified, increasing from bottom to top, we were able to use standard singular perturbation analysis to describe the nature of the transients and the attractors of the system.

Complexed oscillatory behavior is extremely undesirable not only for control and design problems, but also for its potential for dangerous situations which may result in the case where toxic compounds are involved, such as in the operation of toxic waste treatment processes. Insights that can be gained from this type of analysis described above should prove most valuable in the light of such considerations.

ACKNOWLEDGMENT

Appreciation is rendered to the Thailand Research Fund for the financial support which made possible this research project.

REFERENCES

- 1. J. Monod, recherces pur la croessance des cultures bacteriennes, Hermann et Cie, Paris (1942).
- 2. T. Yano. and S. Koga, Dynamic Behavior of the Chemostat Subject to Substrate Inhibition, *Biotechnology and Bioengineering*. 11: 139-153 (1969).
- 3. P. Agrawal, C. Lee, H.C., Lim and D. Ramkrishna, Theoretical Investigations of Dynamic Behavior of Isothermal Continuous Stirred Tank Biological Reactors, *Chemical Engineering Science*. 37(3): 453-462 (1982).
- 4. Lenbury, Y., Novaprateep, B., and Wiwatpataphee, B., Dynamic Behavior Classification of Model for a Continuous Bio-Reactor Subject to Product Inhibition, *Mathl. Comput. Modelling*, 19(12): 107-117 (1994).
- 5. J. Cheng-Fu, Existence and uniqueness of limit cycles in continuos cultures of microorganisms with non-constant yield factor, Universita degli studi di Bari, Italy (Preprint).
- 6. T.Yano and S. Koga, Dynamic Behavior of the Chemostat Subject to Product Inhibition, J. Gen. Appl. Microbiol. 19: 97-114 (1973).
- 7. F. Hoppensteadt, Asymptotic stability in singular perturbation problems II: Problems having matched asymptotic expansions, *J. Differential Equations*. 15:510-512 (1974).
- 8. P.S. Crooke, C.J. Wee and R.D. Tanner, Continuous fermentation model, *Chem. Eng. Commun.* 6: 333-347 (1980).
- 9. S. Muratori, An Application of the Separation Principle for Detecting Slow-Fast Limit Cycles in a Three-Dimensional System, *Appl. Math. and Comput.* 43: 1-18 (1991).
- 10. S. Muratori and S. Rinaldi, Remarks on Competitive Coexistence, SIAM J. APPL. MATH. 49 (5): 1462-1472 (1989).
- 11. S. Muratori and S. Rinaldi, Low- and High-frequency Oscillations in Three Dimensional Food Chain Systems, SIAM J. APPL. MATH. 52(6): 1688-1706 (1992).
- 12. S. Schecter, Persistence unstable equilibria and closed orbits of a singularly perturbed equation, *J. Differential Equations*. 60, : 131-141 (1985).
- 13. A.V. Osipove, G. Soderbacka and T. Eirold, On the Existence of Positive Periodic Solutions in Dynamical System of Two Predator-One Prey Type, *Viniti Deponent n.*4305-B86 [In Russian].

Modelling Effects of High Product and Substrate Inhibition on Oscillatory Behavior in Continuous Bioreactors

MODELLING EFFECTS OF HIGH PRODUCT AND SUBSTRATE INHIBITION ON OSCILLATORY BEHAVIOR IN CONTINUOUS BIOREACTORS

Yongwimon Lenbury*

Apichat Neamvong

Somkid Amornsamankul

Pannee Puttapiban

Department of Mathematics

Faculty of Science, Mahidol University

Rama 6 Rd., Bangkok 10400, Thailand

scylb@mahidol.ac.th

^{*} to whom all correspondences should be addressed.

MODELLING EFFECTS OF HIGH PRODUCT AND SUBSTRATE INHIBITION ON OSCILLATORY BEHAVIOR IN CONTINUOUS BIOREACTORS

ABSTRACT

In this study we consider a model for continuos bioreactors which incorporates the effects of high product and substrate inhibition on the kinetics and biomass and product yields. We theoretically investigate the possibility of various dynamic behavior in the bioreactor over different ranges of operating parameters to determine the delineating process conditions which may lead to oscillatory behavior. Application of the singular perturbation technique allows us to derive explicit conditions on the system parameters which specifically ascertain the existence of limit cycles composed of concatenation of catastrophic transitions occurring at different speeds. We discover further that the interactions between the limiting substrate and the growing microorganisms can give rise to high frequency oscillations which can arise during the transients toward the attractor or during the low-frequency cycle. Such study can not only more fully describe the kinetics in a fermentor but also assist in formulating optimum fermentor operating conditions and in developing control strategy for maintaining optimum productivity.

Key words: continuous bioreactors, product inhibition, substrate inhibition, singular perturbation, oscillation.

NOMENCLATURE

- X concentration of cells in bioreactor, g/ℓ
- S concentration of substrate in bioreactor, g/ℓ
- S_F concentration of substrate in the feeding solution, g/ℓ
- P concentration of product in biorector, g/ℓ
- T time, h
- K_S , K_p positive constants, g/ℓ
- D dilution rate, h-1
- Y yield coefficient, g cell/g substrate
- μ specific growth rate, h-1
- μ_{m} maximum specific growth rate, h-1

INTRODUCTION

The growth of microorganisms is an unusually complicated phenomenon. Viewing the behavior of microbial cultures within the framework of lumped kinetic models, a multitude of models have been proposed and theoretically studied in diverse ways since the model due to Monod [9] fashioned after Michaelis-Menten kinetics for single enzyme-substrate reactions.

In ethanol fermentation, instantaneous biomass yield of the yeast $Saccharomyces\ cerevisiae$ was found by Thatipamala $et\ al.$ in [15] to decrease with the increase in ethanol concentration (P), indicating a definite relationship between biomass yield and product inhibition. It was also found in [15] that substrate inhibition occurs when substrate concentration (S) is above 150 g/ ℓ . Figure 1 shows experimental data taken from the work of Thatipamala $et\ al.$ [15] indicating the effect of substrate inhibition on the specific growth rate at low ethanol concentrations. Figure 2, on the other hand, shows the effect of product inhibition on the specific growth rate, with data taken from the same source [15].

A number of simple kinetic expressions have been suggested in the literature for specific growth rate μ incorporating product and/or substrate inhibition [2-4,16]. Mainly, four types of inhibition correlations have been suggested based on experimental observations: linear, exponential, hyperbolic, and parabolic. In [16], Yano and Koga made a theoretical study on the behavior of a single-vessel continuous fermentation subject to a growth inhibition at high concentration of the rate limiting substrate S. They used the following expression for their continuous fermentation system:

$$\mu = \frac{\mu_{\rm m}}{(K_{\rm s}/S) + 1 + \sum_{\rm j=1}^{\rm n} (S/K_{\rm j})^{\rm j}}$$
(1)

where μ_m and the K's are positive constants and n is a positive integer. Other workers [1,8] have adopted simpler specific growth rate functions involving less control parameters but exhibiting similar necessary characteristics as the usual substrate inhibition model, for example the one hump substrate inhibition function

$$\mu = kSe^{-S/K_s} \tag{2}$$

where k and K_s are positive constants

Later, Yano and Koga discussed in [17] the nature of the chemostat in which the specific growth rate depends on the concentrations of both a substrate and an inhibitory product of a microorganism. They assumed the specific growth rate equation as follows;

$$\mu = \frac{\mu_{\rm m}S}{(K_{\rm s} + S) \left\{ 1 + \left(\frac{P}{K_{\rm p}}\right)^{\rm n} \right\}}$$
(3)

They showed, with the analog computer, that when the product formation was negatively growth-associated, in which the rate of product formation decreases with the increase in the cells concentration, diverging as well as damped oscillations appeared. No oscillations could be observed, on the other hand, when the product formation was either completely growth-associated, or partially growth-associated. Oscillation phenomena are, however, not unusual in continuous cultures [1]. Since such penchant for periodicity is undesirable from the point of view of process control, it is necessary to identify the safe operating regions in which complexed dynamic behavior may be avoided.

In [14], Ramkrishna et al. presented a chemostat model which assumed that viable cells (X) interact with a substrate (S) so as to produce the new viable cells and a cell-killing product (P). This product interacts with viable cells to form dead cells, in the process of which the cell-killing product may be released.

In [8], the dynamic behavior of a chemostat subject to product inhibition was analyzed and classified in terms of multiplicity and stability of steady states and limit cycles. The substrate was assumed to be in sufficient supply so that the model was reduced to a system of two nonlinear differential equations involving only the cells and product concentrations.

In this paper, we consider the full three-variable product inhibition model consisting of the following nonlinear differential equations:

$$\frac{\mathrm{dX}}{\mathrm{dt}} = \mu X - \mathrm{DX} \tag{4}$$

$$\frac{dS}{dt} = D(S_F - S) - \frac{\mu}{Y}X$$
 (5)

$$\frac{dP}{dt} = \eta_0 \mu X + \eta_1 P - DP \tag{6}$$

where X(t) denotes the cells concentration at time t; S(t) the substrate concentration at time t; P(t) the product concentration at time t; S_F the concentration of the feed substrate, while D is the dilution rate at which the feed substrate is being fed into the reactor and the content of the bio-reactor is being removed, and η_0 is the constant for product formation. The term $\eta_1 P$ in equation (6) takes into account the release of the cell-killing product during the product's interaction with viable cells to form dead cells, following the suggestion of Ramkrishna *et al.* in their earlier mentioned paper [14]. Here, we assume that the production rate is directly proportional to the amount of the product present, with $\eta_1 < D$ being the positive constant of variation.

We also adopt the following expression for the specific growth rate function:

$$\mu = \frac{kSe^{-a\frac{S}{S_F}}}{1 + \frac{P}{K_P}} \tag{7}$$

where a and k are positive constants, to take into account the inhibitory effects of both the substrate and the product increase in the chemostat.

Further, the cells to substrate yield Y defined as

$$Y \equiv \frac{\text{amount of cells produced}}{\text{amount of substrate consumed}}$$

is assumed to vary linearly with the substrate level at any time t, allowing for the positively-growth associated situation; namely

$$Y = A + BS \tag{8}$$

Such substrate dependent yield has been used previously by several other workers in this field [1, 8].

The analysis of the model is done through a singular perturbation argument, assuming that the substrate concentration exhibits fast dynamics. The time responses of the different components in the system are assumed to decrease dynamically from top to bottom. The structure of the corresponding attractors and the nature of the transients are then analyzed. It is shown that the model system can exhibit low-frequency cycles in which periodic bursts of high-frequency oscillations may develop giving rise to more complexed dynamical behavior for specified ranges of the system parameters.

SYSTEM MODEL

In order to analyze the model system of equations (4), (5) and (6), together with (7) and (8) through the singular perturbation technique, we assume that the substrate has fast dynamics, while the cells and product have intermediate and slow dynamics respectively, and scale the time responses of the three hierarchical components of the system by means of two small dimensionless positive parameters ϵ and δ ; namely, we let $x = \frac{S}{S_F}$, y = X, $z = \frac{P}{\epsilon K_P}$, $d_1 = D$, $d_2 = \frac{D}{\epsilon}$, $d_3 = \frac{D - \eta_1}{\epsilon \delta}$, $\omega = \frac{kS_F}{\epsilon K_P}$, $\eta = \frac{\eta_0 \omega}{\epsilon \delta}$, $\gamma = \frac{k}{AS_F}$, and $\beta = \frac{A}{BS_F}$. We are led to the following system of differential equations:

$$\frac{dx}{dt} = d_1(1-x) - \frac{\gamma x e^{-ax} y}{(x+\beta)(1+\epsilon z)} = f(x,y,z)$$
 (9)

$$\frac{\mathrm{d}y}{\mathrm{d}t} = \varepsilon y \left[\frac{\omega x \mathrm{e}^{-ax}}{1 + \varepsilon z} - \mathrm{d}_2 \right] = \varepsilon \mathrm{g}(x, y, z) \tag{10}$$

$$\frac{\mathrm{d}z}{\mathrm{d}t} = \varepsilon \delta \left[\frac{\eta x \mathrm{e}^{-\mathrm{a}x}}{1 + \varepsilon z} y - \mathrm{d}_3 z \right] = \varepsilon \delta \mathrm{h}(x, y, z) \tag{11}$$

Thus, with ε and δ small, the equation of the substrate concentration represents the fast system, while that of the cells and product concentrations represent the intermediate and the slow systems, respectively. Under suitable regularity assumptions, the singular perturbation method allows us to approximate the solution of the system (9)-(11) with a sequence of simple dynamic transitions along the various equilibrium manifolds of the system and occurring at different speeds. The resulting path, composed of all such transients, approximates the solution of the system in the sense that the real trajectory is contained in a tube around these transients, and that the radius of the tube goes to zero with ε and δ . The formal proof of this is not given because it is long and trivial and has already been discussed and extensively used in the literature [7,10-12].

Two-dimensional dynamics

By means of singular perturbation analysis, the solution of the system of equations (9)-(11) can be approximately found for small values of ϵ and δ . First, the slow (z) and intermediate (y) variables are frozen at their initial values z(0) and y(0), and the evolution of the fast component of the system is determined by solving the 'fast system' consisting of equation (9) with z set equal to z(0). If, for simplicity of the following analysis, we assume that the starting value of z is comparatively small, since δ is small, the value of z remains small during the initial phase. The evolution of the system components can then be approximately determined by first setting $\delta = 0$ and z = 0 in the equations (9)-(11). Thus, we are led to the following system:

$$\frac{dx}{dt} = d_1(1-x) - \frac{\gamma x e^{-ax} y}{(x+\beta)}$$
 (12)

$$\frac{\mathrm{dy}}{\mathrm{dt}} = \varepsilon y \left[\omega x \mathrm{e}^{-\mathrm{ax}} - \mathrm{d}_2 \right] \tag{13}$$

which is a fast-slow second-order system for which the dynamical behavior can be analyzed and existence of limit cycles detected through the singular perturbation principle. The results are summarized in Figure 3, where two cases of interest can be identified. The conditions on the parameters identifying the two cases are as follows.

Case 1

The system (12) has an equilibrium manifold where $\dot{x} = 0$ given by

$$y = (1 - x)(x + \beta) \frac{e^{ax}}{x} \equiv \phi(x)$$
 (14)

which intersects the x-axis at the point x = 1 as shown in Figure 3. The slope of the curve in (14) is given by

$$\frac{dy}{dx} = \frac{e^{ax}}{x^2} F(x) = \frac{e^{ax}}{x^2} \left[-x^3 + (a - a\beta - 1)x^2 + a\beta x - \beta \right]$$
 (15)

Letting $x = \frac{1}{3}$ in (15) leads to the following inequality

$$\beta < \frac{3a-4}{27-6a} \tag{16}$$

which ensures that the curve $y = \varphi(x)$ has positive slope on some interval containing the point $x = \frac{1}{3}$.

The equilibrium manifold of the intermediate system (13) consists of 2 parts, the trivial manifold y = 0 and the nontrivial manifold given by the equation

$$xe^{-ax} = \frac{d_2}{\omega} \tag{17}$$

In Case 1, the curve (17) intersects the graph of (14) at the point R in the Figure 3 where $x = \overline{x}$ for which

$$F(\bar{x}) > 0 \tag{18}$$

which means that the point R is located on the unstable branch of the manifold f = 0. This is easily accomplished by letting

$$\overline{\mathbf{x}} = \frac{1}{3} - \theta \tag{19}$$

for a sufficiently small θ , then simply set

$$\frac{d_2}{\omega} = \bar{x}e^{-\bar{x}} = (\frac{1}{3} - \theta)e^{-(1/3 - \theta)}$$
 (20)

Thus, Case 1 is identified by the inequality (18) with (19) and (20).

Case 2

This case is then identified by the opposite inequality to (18), namely

$$F(\bar{x}) < 0 \tag{21}$$

However, since the nontrivial intermediate manifold is given by (17),

$$\bar{x} > \frac{d_2}{\omega} \tag{22}$$

We see that (21) will be satisfied if $\frac{d_2}{\omega}$ is sufficiently large as well as satisfying

$$\frac{d_2}{\omega} < 1 \tag{23}$$

to allow for \overline{x} to be located to the left of the point x = 1 where the fast manifold crosses the x-axis.

Thus, in Figure 3 where transitions of low, intermediate, and high speeds are indicated by one, two, and three arrows, respectively, if we start from the point marked by the number 1 above the curve $\dot{x}=0$, then $\dot{x}<0$ here and a fast transition develops toward the point 2 on the stable manifold (section AB), while y still remains frozen at the initial value y(0). (If we start from the point 1 below the curve $\dot{x}=0$, then $\dot{x}>0$ here and so a fast transition will develop toward point 3 on section CD of the manifold). Since the manifold is stable here, a transition of intermediate speed is made along the curve as the intermediate system becomes active. From point 2, the transition develops along the direction of decreasing y since $\dot{y}<0$ on the left of the curve g=0. Once the point B is reached, the manifold loses its stability and a fast transition is made towards the point D on the stable section CD of the manifold. Transition of intermediate speed upwards along this curve ends if either a stable equilibrium R is reached in Case 2, or a quick jump brings the trajectory back to the section AB completing a closed cycle ABDC in Case 1.

Three-dimensional dynamics

As z increases, the slow system (11) becomes active. We now show that, for suitable values of the parameters and for ε and δ sufficiently small, the system (9)-(11) has a unique attractor that is either a stable equilibrium or a low-

frequency limit cycle which may exhibit high-frequency oscillations during a finite interval of time.

To do this, we observe that the manifold

$$f(x,y,z) = 0 (24)$$

intersects the nontrivial intermediate manifold along the curve

$$f = g = 0 \tag{25}$$

given by the equation

$$\frac{xe^{-ax}}{1+\epsilon z} = \frac{d_2}{\omega} \tag{26}$$

which defines a surface $z = \psi(x)$. We observe that at $x = \frac{1}{a}$

$$\frac{\mathrm{dz}}{\mathrm{dx}} = 0$$

Thus, to ensure that the point $P(x_P, y_P, z_P)$ in Fig. 4 is located on the stable part of the manifold f = 0 at the point where $x_P = \frac{1}{a} < 1$, we require

$$F\left(\frac{1}{a}\right) < 0 \tag{27}$$

or equivalently,

$$\beta > 1 - \frac{1}{a} - \frac{1}{a^2} \tag{28}$$

and

$$a > 1 \tag{29}$$

Combining the inequalities (16) and (28), we arrive at the requirement that

$$\frac{3a-4}{27-6a} > \beta > 1 - \frac{1}{a} - \frac{1}{a^2} \tag{30}$$

Now, the curve (25) is given by the equation

$$y = \frac{d_2}{\omega}(1-x)(x+\beta)$$

which reaches a maximum at the point $M(x_M, y_M, z_M)$ where

$$x_{M} = \frac{1-\beta}{2}$$

Finally, the curve f = g = 0 intersects the (x,z)-plane at the point $O(x_0,y_0,z_0)$ where $x_0 = 1$ and, from (26),

$$z_{o} = \frac{1}{\varepsilon} \left(\frac{\omega}{d_{2}e^{a}} - 1 \right) \tag{31}$$

We therefore require that

$$e^{a} < \frac{\omega}{d_{2}} \tag{32}$$

to ensure that $z_0 > 0$.

We now analyze each of the two cases separately.

Case 1

We observe that in this case the point R is located on the unstable part of the manifold f = 0 and the curve f = g = 0 remains on the unstable part, as shown in Figure 4, until the point M is reached. The curve then stretches along the stable part of the manifold f = 0 until either the point S is reached in the cases 1(a) and 1(b), or the point P is reached first in the cases 1(c) and 1(d). Thus, four subcases can be identified as follows.

<u>Case1(a)</u> This case is identified by the inequality

$$a < 1 \tag{33}$$

so that the turning point P is below the (x,z)-plane. Thus, starting from an initial point A in Figure 4, a fast transient takes us to the point B on the stable part of the fast manifold f = 0. Transition of intermediate speed is then made along this manifold in the direction of increasing y until the point C is reached where stability is lost. A fast jump is made to the point D on the other stable branch of the manifold f = 0 from which point a transition of intermediate speed develops until stability is lost again at the point G. A quick jump back to H almost closes up the cycle. However, z has been slowly increasing in the meantime so that the same cycling transitions are repeated in the direction of increasing z, densely covering the surface f = 0, until the point M is reached. The transient now follows the curve f = g = 0 until the point S is reached in the case f = 0. In this case, the point S where f = 0 is on the stable part of the manifold f = 0 and thus the transitions end at this stable equilibrium point.

Case 1(b) This is the case identified by the inequality

$$a > 1 \tag{34}$$

so that the point P is located on f = 0 above the (x,z)-plane as shown in Figure 4 (b). This case is also identified by the fact that the point S, where f = g = h, is located on the stable part of the curve f = g = 0. This situation is guaranteed by requiring that

$$z_{P} > z_{N} \tag{35}$$

where $N(x_N, y_N, z_N)$ is the point on the curve f = h = 0 with $x_N = \frac{1}{a}$. From equating f and h to zero, we find that

$$z_{N} = \frac{\eta d_{1}}{\gamma d_{3}} \left(1 - \frac{1}{a} \right) \left(\frac{1}{a} + \beta \right) \tag{36}$$

while, from equation (26), we have

$$z_{P} = \frac{1}{\varepsilon} \left(\frac{\omega}{\text{aed}_{2}} - 1 \right) \tag{37}$$

Therefore, so that S is located on the stable part of f = g = 0, we require

$$\frac{\omega}{d_2} > ae \left[\frac{\varepsilon \eta d_1}{\gamma d_3} \left(1 - \frac{1}{a} \right) \left(\frac{1}{a} + \beta \right) + 1 \right]$$
 (38)

which guarantees that (35) holds.

In this case 1(b) then, the transition also reaches the point S first and ends there since it is a stable equilibrium point where $\dot{x} = \dot{y} = \dot{z} = 0$. Moreover, along The curve f = h = 0 we have

$$z = \frac{\eta d_1}{\gamma d_3}$$

when x = 0. Therefore we must also require that

$$\frac{\eta d_1 \beta}{\gamma d_3} > \frac{1}{ae} \tag{39}$$

to ensure that the curve f = h = 0 intersects the curve f = g = 0 only once.

Case 1(c) This case is identified by inequality (34) and the opposite inequality to (38), that is

$$\frac{\omega}{d_2} < ae \left[\frac{\varepsilon \eta d_1}{\gamma d_3} \left(1 - \frac{1}{a} \right) \left(\frac{1}{a} + \beta \right) + 1 \right]$$
 (40)

which guarantees that the point P is reached first during the transition from the point M in Figure 4(c). At the point P, there is a loss of stability and a quick jump to E takes place. A slow transition develops now along this manifold where x = 1 until a point is reached where stability in again lost at some point F. A transition of intermediate speed will develop along the fast manifold f = 0 back to the point L which completes the limit cycle in the case 1(c).

Case 1(d) In order that the transition goes back into high-frequency oscillations in each low-frequency cycle, we need to require that $z_0 < z_M$, which is equivalent to

$$e^{-a} < \frac{1-\beta}{2}e^{-a(1-\beta)/2}$$
 (41)

Thus, starting from the point A in Figure 4(d), a fast transition takes us, as explained earlier, to the point B on f = 0. An intermediate transition develops on this manifold until C is reached where the stability of the equilibrium fast manifold is lost. A fast transition then takes the system to the stable equilibrium point D. An intermediate speed transition is then made along this branch of manifold until G is reached where the stability is again lost and a quick jump brings us to the stable point H. This almost closes up the cycle but just misses the point B. The slow system has becomes active and z has been slowly increasing since $\dot{z} > 0$ here. Transitions then develop following the same pattern but with slowly varying z as seen in Figure 4(d) until M is reached, at which point the trajectory develops into a slow cycle which goes back into the fast cycles since inequality (41) guarantees that $z_0 < z_M$.

Case 2

We observe that in this case the point R is located on the stable part of the fast manifold f = 0 as shown in Figure 5. Mainly 3 subcases can therefore be identified here.

Case 2(a) If (21) as well as (33) hold then starting from the point A in Figure 5(a), a fast transition develops to the point B, followed by a transient of intermediate speed to C, from which point a slow transient takes us to the stable equilibrium point S where the transition ends.

Case 2(b) If (21) holds as well as (38) then, similarly to Case 2(a), transients develop toward the stable equilibrium point S where $\dot{x} = \dot{y} = \dot{z} = 0$ and the transition ends.

Case 2(c) Finally, if (21) holds as well as (40) then, from the point C in Figure 5(c), the point P is reached first where the stability is lost. A quick jump to E, followed by a transition at slow speed from E to F, then at intermediate speed back to D, closes the trajectory up into a low-frequency limit cycle for this case 2(c).

The above analysis can be summarized by the following theorem.

Theorem If ε and δ are sufficiently small, and if (16), (30), (32), and (39) hold, then system (9)-(11) has a global attractor which is a stable equilibrium if (18) and (33) hold, or (18), (34) and (38) hold, or if (21) and (33) or (38) hold. It is a low-frequency limit cycle if (21) and (40) hold, or if (18), (34) and (40) hold. Moreover, if (18), (34) and (40) as well as (41) hold, then the attractor is a low-frequency limit cycle which contains a period of high frequency oscillations.

NUMERICAL RESULTS AND DISCUSSION

Figure 6(a) shows a numerical simulation of the model equations (9)-(11) with parametric values chosen to satisfy inequalities (18), (30), (32), (34), (39) and (40). This is therefore the case 1(c) and the solution trajectory develops into a low-frequency limit cycle as predicted. The corresponding time courses of the three variables are shown in Figure 7(a).

Figure 6(b) shows a numerical simulations of the model equations (9)-(11) with parametric values chosen to satisfy inequalities (18), (30), (32), (34), (39), (40) as well as (41). This is therefore Case 1(d). The solution trajectory develops into a low-frequency limit cycle which contains high frequency oscillations as predicted in the above theorem. The corresponding time courses of the three variables are shown in Figure 7(b). Such underlying high frequency cycles in the biomass concentration profile have frequently been observed by a number of investigators [16-18]. In [16], the total budding cells count in their bioreactor data shows oscillatory behavior closely resembling our result of case 1(d) shown in Figure 7(b). Experimenting with different values for the system parameters such as β , d₃, a, and so on, shows that the frequencies and amplitude of oscillations can be appropriately adjusted to fit different chemostat conditions.

We observe that the constant a plays an important role in the kinetics of the chemostat under study. Considering the model in equation (7), a is in fact an indicator of how late or how soon the substrate inhibition sets in. In Figure 1, substrate inhibition seems to set in approximately half way to the maximum substrate level, suggesting that a should by around 2. Thus, the numerical results presented in Figures 6(a) and 6(b) can be considered as corresponding to the case where substrate inhibition is late in setting in (a < 2). In Figure 6(c), we present a numerical simulation of equations (9)-(11) in which a = 2.5, thus corresponding to the situation where the inhibition sets in rather early (a > 2). With this value of a, inequality (32) is violated and a = 2.5. Therefore, the transition develops from the

point E (in Figure 4(c) or 5(c)) all the way to the point (1, 0, 0) on the x-axis which is a stable washout steady state of the system. Figure 7(c) shows the corresponding time courses of the state variables in this case, where both the cells and product levels are seen to decrease toward zero, while the substrate level tends toward the maximum level $(S = S_F)$.

Also, it is numerically found that solution trajectories can still develop as theoretically predicted even though the values of ϵ and δ are not so small, and the assumption that the three components of the system carry highly diversified dynamics can be relaxed to a certain extent.

CONCLUSION

The appearance of sustained oscillations in bioreactor variables in continuous cultures indicates the complex nature of microbial systems, and the difficulties which may arise in bioprocess control and optimization.

In this paper, the dynamic behavior of a continuous bioreactor described by equations (9)-(11) has been investigated, incorporating the inhibitory effect at high levels of product and substrate concentrations. Assuming that the time responses of the three components are highly diversified, increasing from bottom to top, we were able to use standard singular perturbation analysis to describe the nature of the transients and the attractors of the system.

Complexed oscillatory behavior is extremely undesirable not only for control and design problems, but also for its potential for dangerous situations which may result in the case where toxic compounds are involved, such as in the operation of toxic waste treatment processes. Insights that can be gained from this type of analysis described above should prove most valuable in the light of such considerations.

ACKNOWLEDGMENT

Appreciation is rendered to the Thailand Research Fund for the financial support which made possible this research project.

FIGURE CAPTIONS

- FIGURE 1. Effect of substrate inhibition on specific growth rate at low ethanol concentration. (Data points taken from reference [15]).
- FIGURE 2. Effect of product inhibition on specific growth rate. (Data points taken from reference [15]).
- FIGURE 3. Two possible cases of trajectory development for the two dimensional fast-slow system (12), (13). Trajectories go toward a limit cycle ABDC in Case 1, and toward a stable equilibrium point R in Case 2.
- FIGURE 4. Trajectories of the model system (9)-(11) in Case 1 exhibiting four possible subcases 1(a), 1(b), and 1(c) identified in the text.
- FIGURE 5. Trajectories of the model system (9)-(11) in Case 2 exhibiting three possible subcases 2(a), 2(b), and 2(c) identified in the text.
- FIGURE 6. Numerical simulation of the model equations (9)-(11). Here, $\epsilon = 0.1$, $\delta = 0.01$, $\gamma = 2.0$, $\eta = 10.0$, $\omega = 3.0$, $d_1 = 0.25$, $d_2 = 0.25$, and $d_3 = 0.1$. In 6(a), the parametric values satisfy the inequalities of Case 1(c), with $\beta = 0.8$, a = 1.5, and the solution trajectory tends toward a low-frequency limit cycle as theoretically predicted. In 6(b), the parametric values satisfy the inequalities of Case 1(d), with $\beta = 0.2$, a = 1.5, and the solution trajectory tends toward a low-frequency limit cycle which contains a period of high-frequency oscillations. In 6(c), $\beta = 0.2$, and $\alpha = 0.2$, which corresponds to the situation where substrate inhibition is early in setting in.
- FIGURE 7. The time courses of the state variables x(t), y(t) and z(t) are shown here corresponding to the three respective cases seen in Figure 6.

 represents x(t) + 2.2 in 7(a), x(t) + 0.4 in 7(b), and x(t) in 7(c).

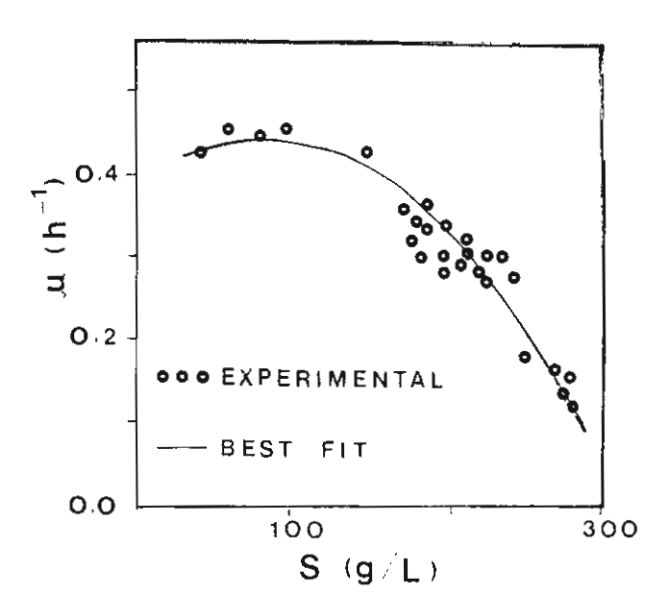
 o—o represents y(t).

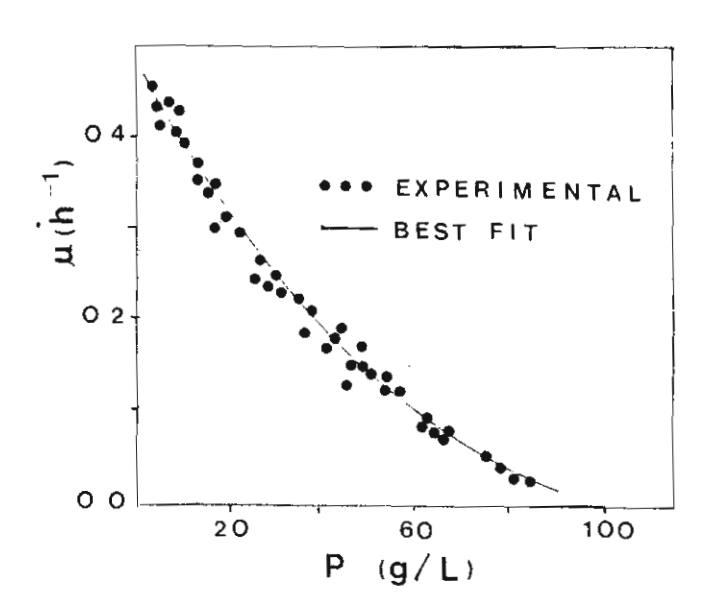
 ×—× represents z(t) + 0.3 in z(t) in z(t) in z(t) and z(t) in z(t) and z(t).

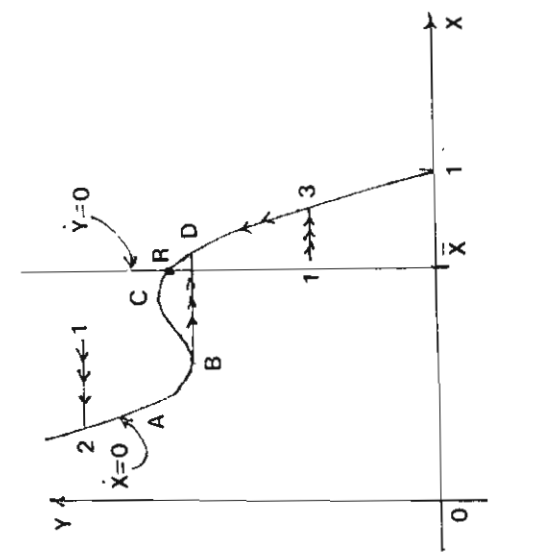
REFERENCES

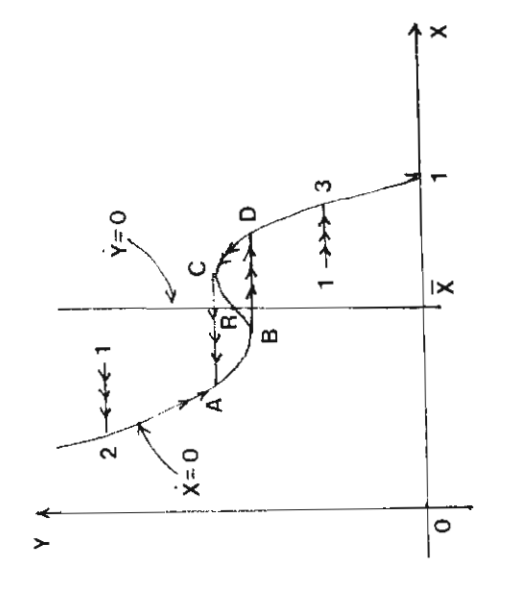
- 1. Agrawal, P., Lee, C., and Lim, H.C.: and Ramkrishna, D., Theoretical Investigations of Dynamic Behavior of Isothermal Continuous Stirred Tank Biological Reactors. *Chemical Engineering Science*. 37 (1982)3, pp. 453-462.
- 2. Aiba, S., and Shoda, M.: Reassesment of the product inhibition of alcohol fermentation. *J. Ferment. Technol.* 47 (1969) pp. 790-799.
- 3. Andrews, J. F.: A mathematical model for the continuous culture of microorgnisms utilizing inhibitory substrates. *Biotechnology and Bioengineering*. **10** (1968) pp. 707-723.
- 4. Bazua, C. D., and Wilke, C. R.: Ethanol effects on the kinetics of a continuous fermentation with Saccharomyces cerevisiae. Biotechnology and Bioengineering Symp. 7 (1977) pp. 105-118.
- 5. Ching-I Chen, and McDonald, K. A.: Oscillatory Behavior of *Saccharomyces cerevisiae* in Continuous Culture: I Effects of pH and Nitrogen Levels. *Biotechnology and Bioengineering*. **36** (1990) pp. 19-27.
- Ching-I Chen, and McDonald, K. A.: Oscillatory Behavior of Saccharomyces cerevisiae in Continuous Culture: II Analysis of Cell Synchronization and Metabolism. Biotechnology and Bioengineering. 36 (1990) pp. 28-38.
- 7. Hoppensteadt, F.: Asymptotic stability in singular perturbation problems II: Problems having matched asymptotic expansions. *J. Differential Equations.* 15 (1974) pp. 510-512.
- 8. Lenbury, Y., Novaprateep, B. and Wiwatpataphee, B.: Dynamic Behavior Classification of a Model for a Continuous Bio-Reactor Subject to Product Inhibition. *Mathl. Comput. Modelling.* 19 (1994) 12, pp. 107-117.
- 9. Monod, J.: recherces pur la croessance des cultures bacteriennes, Hermann et Cie, Paris, 1942.

- Muratori, S.: An Application of the Separation Principle for Detecting Slow-Fast Limit Cycles in a Three-Dimensional System. Applied Mathematics and Computation. 43 (1991) pp. 1-18.
- 11. Muratori, S. and Rinaldi, S.: Remarks on Competitive Coexistence, SIAM J. APPL. MATH. 49 (1989) 5, pp. 1462-1472.
- Muratori, S. and Rinaldi, S.: Low- and High-frequency Oscillations in Three Dimensional Food Chain Systems. SIAM J. APPL. MATH. 52 (1992) 6, pp. 1688-1706.
- Olsvik, E. S., and Kristiansen, B.: Influence of Oxygen Tension, Biomass Concentration, and Specific Growth Rate on the Rheological Properties of a Filamentous Fermentation Broth. *Biotechnology and Bioengineering*. 40 (1992) pp. 1293-1299.
- 14. Ramkrishna, D., Fredrickson, A.G., and Tsuchiya, H.M.: Dynamics of Microbial Propagation: Models Considering Inhibitors and Variable Cell Composition, *Biotech. Bioeng.* 9 (1967) p. 129-170.
- Thatipamala, R., Rohani, S., and Hill, G. A., Effects of High Product and Substrate Inhibitions on the Kinetics and Biomass and Product Yields During Ethanol Batch Fermentation, *Biotechnology and Bioengineering*. 40 (1992) pp. 289-297.
- 16. Yano, T., and Koga, S.: Dynamic Behavior of the Chemostat Subject to Substrate Inhibition. *Biotechnology and Bioengineering*. 11 (1969) pp. 139-153.
- 17. Yano, T. and Koga, S.: Dynamic Behavior of the Chemostat Subject to Product Inhibition. J. Gen. Appl. Microbiol. 19 (1973) pp. 97-114.









CASE 2

CASE 1

, -

